Chain level insights into tensile-compressive asymmetry in glassy and semicrystalline polymers

Sara Jabbari-Farouji 1,* and Damien Vandembroucq 2 *,†

^{†1} Institute of Physics, Johannes Gutenberg-University, Staudingerweg 7-9, 55128 Mainz, Germany

² Laboratoire PMMH, UMR 7636 CNRS/ESPCI Paris/Universite Pierre et Marie Curie/Universite Paris Diderot

E-mail: sjabbari@uni-mainz.de

Abstract

Using molecular dynamics simulations, we provide chain-level insights into the dissimilarities in rearrangements of polymers under uniaxial tensile and compressive deformation in glassy and semicrystalline samples of varying chain lengths. The organization of polymers under tension and compression is distinctively different. The chains align themselves along the tensile axis leading to a net global nematic ordering of their bonds and end-to-end vectors whereas under compression, the polymers arrange themselves in a plane perpendicular to the compressive axis resulting in emergence of an anti-nematic ordering of the bonds and the chain end-to-end vectors. Moreover, the degree of polymers unfolding is greater under tension and they deform less affinely when compared to chains under compression. The difference between the two responses strongly depends on the chain length and is the largest at intermediate chain lengths.

Solid-like polymers used in various highperformance products are subjected to various loading conditions, *e.g.* tensile and compression. The mechanical response of a polymeric material not only depends on its structure but also on the imposed deformation mode.^{1,2} For instance, the compressive yield strengths of polycarbonate and polymethylmethacrylate polymer glasses are about 20% larger than their tensile yield strength.^{3,4} Therefore, understanding the link between the deformation-dependent response and the underlying structural rearrangements is crucial for a bottom-up design of polymeric materials with desired mechanical properties.

The mechanical responses of glassy and semicrystalline polymers under various deformation modes have been the subject of intensive experimental and theoretical investigations.^{4–21} However, the effect of deformation mode on conformational and structural arrangement of polymers, especially in the strain-hardening regime, has received much less attention .^{5,12,15,22} Gaining chain-level insights into deformation mechanisms of polymers is experimentally challenging due to the small length scales involved. Molecular simulations allowing a direct access to various intrachain and interchain statistical measures have played an important role in illuminating the underlying mechanisms of plastic flow in polymeric solids.^{7,14–17,19,21,23,24}Nonetheless, very few of them have focused on the role of deformation mode on these rearrangements.^{15,22} Moreover, these studies have used atomistic simulations

that are limited to small samples due to their high computational costs. For instance, molecular simulations investigating the dependence of deformation mode in semicrystalline polymers focused only on a layered semicrystalline morphology as part of a larger spherulite structure.¹⁵ Therefore, the underlying differences in microstructural arrangements of polymers under various deformation modes and particularly the effect of chain length is poorly understood.

To make a headway in this direction, we use large-scale molecular dynamics (MD) simulations of a crystallizable bead-spring model²⁵ that allows us to generate large samples including up to 2×10^6 monomers. This model is known as the coarse-grained polyvinyle alcohol (CG-PVA) 25,26 with a distinctive feature of triple-well bending potential. Upon slow cooling of its melt, chains undergo a crystallization transition and form chain-folded structures consisting of randomly oriented crystallites with 2D hexagonal order immersed in a network of amorphous strands. For a rapid quench, polymers retain their amorphous configurations and undergo a glass transition.^{19,21} A prior investigation of tensile response of both amorphous and semicrystalline polymers²¹ showed that the response of long polymer glasses is dominated by the entanglement network whereas that of semicrystalline polymers is determined by an interplay of the two interpenetrated networks of entanglements and tie chains.²¹ Here, we focus on the asymmetry between the tensile and compressive responses of glassy and semicrystalline polymers.

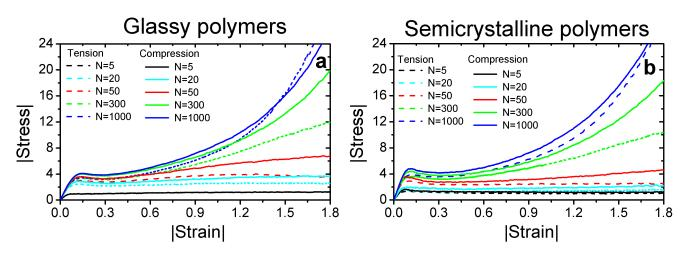


Figure 1: The magnitude of true stress in units of $\epsilon_{\rm LJ}/\sigma^3$ versus true strain from uniaxial compression (lines) and tensile (circles) deformation of (a) glassy and (b) semicrystalline polymers with chain lengths N = 5, 20, 50, 300 and 1000 as given in the legends.

MD simulations were performed using LAMMPS.²⁷ A bead-spring model with a triple-well bending potential is used.^{26,28} Distances are reported in units of $\sigma = 0.52$ nm, the bond length is $b_0 = 0.5\sigma$. A 6-9 Lennard-Jones potential is used to model the non-bonded interactions with the range and strength $\sigma_{\rm LJ} = 0.89\sigma$ and $\epsilon_{\rm LJ} = 1.511 k_B T_0$ where $T_0 = 550$ K is the reference temperature.²⁵ The Lennard-Jones potential is truncated and shifted at $r_c = 1.6\sigma$. Temperatures $T = T_{real}/T_0$ and pressures $P = P_{real}\sigma^3/\epsilon$ are reported in reduced units.

Glassy and semicrystalline samples of different chain lengths, N = 5, 20, 50, 300 and 1000, see ²⁹ for more details, are obtained from cooling melts at T = 1 to T = 0.2 by cooling-rates $\dot{T} = -10^{-3} \tau^{-1}$ and $\dot{T} = -10^{-6} \tau^{-1}$, respectively. The polymer gyration radii span from length scales comparable to monomers size for N = 5 to much larger than the entanglement length in the melt $N_e \approx 36.^{26}$ The samples are deformed in the *y*-direction with a constant true strain-rate of $\dot{\varepsilon} = \pm 10^{-5} \tau^{-1}$ while imposing a constant pressure P = 8 (as in the undeformed samples) in the x and z-directions. The volume increase is at most 10 % for both glassy and semicrystalline polymers at the largest strain $|\varepsilon| = 1.8$ and $T = 0.2^{-29}$ and these systems behave nearly as an incompressible fluid for $|\varepsilon| < 1.$

Figures 1a and b present stress-strain curves

for glassy and semicrystalline polymers obtained under compressive and tensile deformation, respectively. For all the samples, the elastic regime at small strains is followed by a plastic flow at larger deformations. For the shortest chain length N = 5 with $R_g \approx 0.7\sigma$, we observe a stress plateau beyond the yield point and the compressive and tensile responses of both glassy and semicrystalline polymers are almost identical. For longer polymers, the stress response is larger in compression than in tension. The asymmetry is most pronounced at intermediate chain lengths N = 50 and 300. Interestingly, for the longest chain length N = 1000, the compressive and tensile responses become similar again.

To gain insights into chain rearrangements under macroscopic deformation, we measure the RMS components R_i of the end-to-end vectors of chains as relative to their initial values R_0^{α} .⁷ The effective microscopic stretch ratio is defined as $\lambda_{eff} \equiv \sqrt{\frac{\langle R^{y^2} \rangle}{\langle R_0^{y^2} \rangle}}$ where the *y*-direction is taken as the tensile/compressive axis. Under an affine uniaxial compressive or tensile deformation, λ_{eff} is identical to the macroscopic stretch ratio obtained as $\lambda \equiv L_y/L_y^0$ and the changes in $\langle R^{\alpha^2} \rangle$ are consistent with a volume conserving uniaxial macroscopic deformation, *i.e.*, $\lambda_{eff} = \frac{\langle R_0^{x^2} \rangle}{\langle R^{x^2} \rangle}$ $= \frac{\langle R_0^{z^2} \rangle}{\langle R^{z^2} \rangle}.$ The ratio λ_{eff} has recently been identified as an important

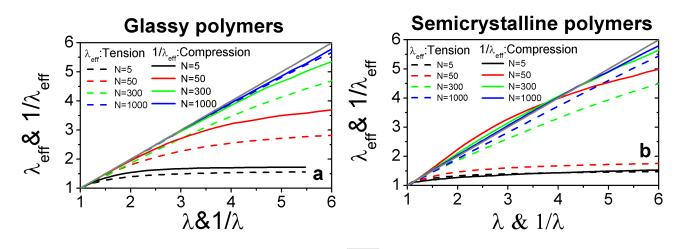


Figure 2: Effective microscopic stretch $\lambda_{eff} \equiv \sqrt{\frac{\langle R_y^2 \rangle}{\langle R_y^0 \rangle}}$ versus macroscopic stretch $\lambda \equiv L_y/L_y^0$ for samples under tension (dashed lines) and $1/\lambda_{eff}$ versus $1/\lambda$ for polymers under compression (solid lines) in (a) glassy and (b) semicrystalline polymers with different chain lengths as given in the legends.

parameter controlling the strain hardening behavior of amorphous and semicrystalline polymers^{7,21} in the sense that, independently of the chain lengths, when $\lambda_{eff}(\lambda)$ of two samples are similar, their responses in the strain-hardening regime are also alike.

Figures 2a and b display λ_{eff} as a function of the macroscopic stretch λ for tensile measurements and $1/\lambda_{eff}$ versus $1/\lambda$ for compressive tests of glassy and semicrystalline polymers, respectively. Similar to the results for tensile deformation, ²¹ under compression polymers in semicrystalline state deform less affinely than their glassy counterparts. The general trend that we observe is that the longer chains exhibit a more affine behavior irrespective of deformation mode and their underlying structure. Overall, polymers deform more affinely under compression than under tension. Notably, the effective microscopic stretch reflects well the compressive-tensile asymmetry observed in the stress-strain curves in Fig. 1. The difference between λ_{eff} in the tensile deformation and $1/\lambda_{eff}$ in the compression is large when the asymmetry between the two responses is significant.

To directly quantify the evolution of the average chain conformations under deformation, we compute the intrachain orientational bondbond correlation function. It is defined as $\langle \cos \theta(n) \rangle \equiv \langle \hat{\mathbf{b}}_{i,j} \cdot \hat{\mathbf{b}}_{i,j+n} \rangle$ where $\hat{\mathbf{b}}_{i,j}$ denotes the orientation vector of the *j*th bond in the *i*th chain and $1 \leq n \leq N-1$ is the curvilinear distance between any two monomers in a chain. Fig. 3 represents $\langle \cos \theta(n) \rangle$ at different stages of compressive and tensile deformations for glassy and semicrystalline samples with chain lengths N = 50 and N = 1000. Upon increase of strain and chain unfolding, the intrachain orientational correlation length grows regardless of the initial structure and deformation mode. Nonetheless, under identical conditions the degree of chain unfolding in the tensile deformation is larger compared to the compression.

We next examine the collective organization of the chains. To this end, we calculate the nematic order tensor of all the chain end-toend orientation vectors $\widehat{\mathbf{R}}_i$ obtained as $\mathbf{Q} = \frac{1}{2n_c} \sum_{i=1}^{n_c} (3\widehat{\mathbf{R}}_i \widehat{\mathbf{R}}_i - \mathbf{I})$ where n_c is the the number of chains in a sample. We define S_{ee} as the eigenvalue of \mathbf{Q} with the largest magnitude varying in the range $-0.5 \leq S_{ee} \leq 1$. In the isotropic case, the three eigenvalues are null and $S_{ee} = 0$. The degeneracy is lifted as soon as the structure gets anisotropic. Two extreme cases can be considered. When all the end-toend vectors are aligned in the same direction, $S_{ee} \rightarrow 1$ leading to a perfect uniaxial nematic alignment. On the other hand, when all the

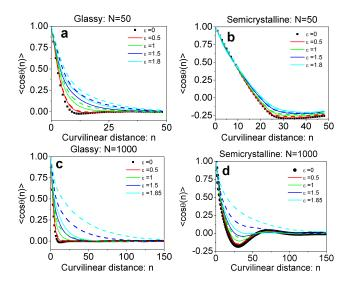


Figure 3: Evolution of intrachain bond-bond orientational correlation function $\langle \cos \theta(n) \rangle$ against the curvilinear distance *n* plotted at different stages of compressive (solid lines) and tensile (dashed lines) deformation for glassy and semicrystalline polymers with chain lengths N = 50 and 1000. The strain magnitudes ε are given in the legends.

end-to-end vectors are perpendicular to a direction, a uniaxial anti-nematic order charactrized by $S_{ee} \rightarrow -0.5$ emerges. Fig. 4a and b show the evolution of S_{ee} as a function of strain for glassy and semicrystalline polymers, respectively. Under tensile deformation, the chains end-to-end vectors get aligned along the tensile axis and S_{ee} progressively increases with strain, approaching unity at large strains. On the contrary under compression where the strain is negative, S_{ee} becomes gradually more negative and it approaches -0.5 already at $\varepsilon \approx -1.5$ for N > 5. This anti-nematic ordering reflects a distinct arrangement of chains under compression. As they are compressed in one direction, the chains elongate isotropically in directions perpendicular to the compressive axis, and their end-toend vectors lie in a plane normal to the deformation axis. Likewise, we define $S_{\text{all-bond}}$ as the largest magnitude eigenvalue of the global nematic tensor of all the bond orientation vectors $\mathbf{Q} = \frac{1}{2n_{\text{bond}}} \sum_{i=1}^{n_{\text{bond}}} (3\widehat{\mathbf{b}}_i \widehat{\mathbf{b}}_i - \mathbf{I})$ where n_{bond} is the the number of all the bonds in a sample. Investigating the global nematic order parameter of the bond vectors $S_{\text{all-bond}}$ presented in

5

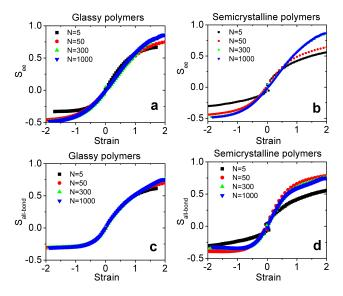


Figure 4: The nematic order parameter of chains end-to-end vector, S_{ee} for glassy (a) and semicrystalline (b) polymers of different chain lengths, N, as a function of strain in both compression (negative strain) and tensile deformation modes. Likewise, the strain-dependence of the global nematic order parameter of all bonds, $S_{\rm all-bond}$, for glassy (c) and semicrystalline (d) polymers.

Fig. 4c and d, we observe a very similar trend; nematic ordering under tensile deformation and anti-nematic ordering under compressive deformation.

Our results highlight the distinct nature of inter- and intra-chain organization in glassy and semicrystalline polymers under compressive and tensile deformations. In both cases, the initial hexagonal order of semicrystalline polymers is destroyed at large deformations and the configurations of semicrystalline and glassy polymers become similar. Under tension, the chain end-to-end vectors and the bond vectors of all the samples align themselves along the deformation axis leading to a net nematic ordering whereas under compression a novel antinematic ordering emerges as a result of chain unfolding. Such an anti-nematic ordering suggests that a buckling-like mechanism may be at play under compression as supported by visual inspections and distribution of bond angles.²⁹ The two responses become similar for very short and long chains, whereas the asymmetry is maximum at intermediate chain lengths.

As mentioned earlier, short chains behave like monomers. Upon increase of chain length beyond the entanglement length $N_e \approx 36$, an entanglement network builds up in glassy polymers. In semicrystalline polymers, part of the entanglement network is lost but instead a network of tie chains connecting the crystalline domains is developed where the average tie-chain length varies in the range $10 < L_{\rm tie} < 30$ for $50 \leq N < 1000.^{21}$ Hence, the longest chains N = 1000 generate long enough tie chains comparable to their entanglement length $N_e \approx 40$ 30 that enforce affine deformation at the chain level whereas intermediate chain lengths deform non-affinely. The effect of deformation mode on the entanglement network structure and the distribution of entanglement points along the chains remains an open question that merits future investigations.

Acknowledgement S. J.-F. acknowledges financial support from the German Research Foundation (http://www.dfg.de) within SFB TRR 146 (http://trr146.de). The computations were performed using the Froggy platform of the CIMENT infrastructure supported by the Rhone-Alpes region (Grant No. CPER07-13 CIRA) and the Equip@Meso Project (Reference 337 No. ANR-10-EQPX-29-01) and the supercomputer clusters Mogon I and II at Johannes Gutenberg University Mainz (hpc.unimainz.de).

References

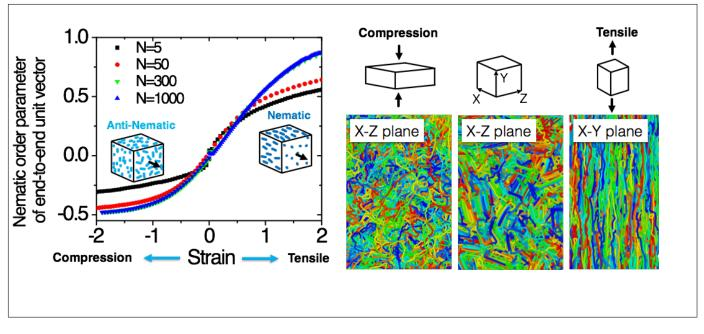
- Ward, I. M.; Sweeney, J. Mechanical Properties of Solid Polymers; 3rd ed., Wiley, Chichester, UK, 2013.
- (2) Roesler, J.; Harders, H.; Baeker, M. Mechanical Behavior of Engineering Materials. Metals, Ceramics, Polymers, and Composites; Springer, Berlin., 2007.
- (3) Inoue, N.; Yonezu, A.; Watanabe, Y.; Yamamura, H.; Xu, B. ASME. J. Eng. Mater. Technol. 2017, 139(2), 021002– 021002.
- (4) Senden, D. J. A.; van Dommelen, J. A. W.;

Govaert, L. E. Journal of Polymer Science Part B: Polymer Physics **2010**, 48, 1483– 1494.

- (5) Boyce, M. C.; Arruda, E. M. Polymer Engineering & Science 1990, 30, 1288–1298.
- (6) Rottler, J.; Robbins, M. O. *Phys. Rev. E* 2003, 68, 011507.
- (7) Hoy, R.; Robbins, M. O. *Physical Review Letters* 2007, *99*, 117801.
- (8) Men, Y.; Rieger, J.; Strobl, G. Phys. Rev. Lett. 2003, 91, 095502.
- (9) Humbert, S.; Lame, O.; Vigier, G. Polymer 2009, 50, 3755 – 3761.
- (10) Lin, P.; Cheng, S.; Wang, S.-Q. ACS Macro Letters 2014, 3, 784–787.
- (11) Liu, J.; Lin, P.; Cheng, S.; Wang, W.; Mays, J. W.; Wang, S.-Q. ACS Macro Letters 2015, 4, 1072–1076.
- (12) Tervoort, T. A.; Govaert, L. E. Journal of Rheology 2000, 44, 1263–1277.
- (13) Jatin,; Sudarkodi, V.; Basu, S. International Journal of Plasticity 2014, 56, 139 155.
- (14) Lee, S.; Rutledge, G. C. Macromolecules 2011, 44, 3096–3108.
- (15) Kim, J. M.; Locker, R.; Rutledge, G. C. Macromolecules 2014, 47, 2515–2528.
- (16) Yeh, I.-C.; Andzelm, J. W.; Rutledge, G. C. *Macromolecules* **2015**, *48*, 4228–4239.
- (17) Oleinik, E. F.; Mazo, M. A.; Strelnikov, I. A.; Rudnev, S. N.; Salamatina, O. B. *Polymer Science, Series A* **2018**, 60, 1–49.
- (18) van Dommelen, J.; Parks, D.; Boyce, M.; Brekelmans, W.; Baaijens, F. Journal of the Mechanics and Physics of Solids 2003, 51, 519 - 541.

- (19) Jabbari-Farouji, S.; Rottler, J.; Lame, O.; Makke, A.; Perez, M.; Barrat, J. L. ACS Macro Letters 2015, 4, 147–151.
- (20) Jabbari-Farouji, S.; Rottler, J.; Lame, O.; Makke, A.; Perez, M.; Barrat, J. L. Journal of Physics: Condensed Matter 2015, 27, 194131.
- (21) Jabbari-Farouji, S.; Lame, O.; Perez, M.; Rottler, J.; Barrat, J.-L. *Phys. Rev. Lett.* 2017, 118, 217802.
- (22) Strelnikov, I. A.; Mazo, M. A.; Balabaev, N. K.; Oleinik, E. F.; Berlin, A. A. *Dokl. Phys. Chem.* **2014**, 457, 108.
- (23) Cho, H.; Weaver, J. C.; Poeselt, E.; in't Veld, P. J.; Boyce, M. C.; Rutledge, G. C. Advanced Functional Materials 2016, 6938–6949.
- (24) Parker, A. J.; Rottler, J. ACS Macro Letters 2017, 6, 786–790.
- (25) Meyer, H.; Muller-Plathe, F. The Journal of Chemical Physics 2001, 115, 7807– 7810.
- (26) Jabbari-Farouji, S. Journal of Polymer Science Part B: Polymer Physics 2018, 56, 1376–1392.
- (27) Plimpton, S. Journal of Computational Physics 1995, 117, 1–19.
- (28) Meyer, H.; Muller-Plathe, F. Macromolecules 2002, 35, 1241–1252.
- (29) Jabbari-Farouji, S.; Vandembroucq, D. Supporting information
- (30) Luo, C.; Sommer, J. ACS Macro Letters 2013, 2, 31–34.

Graphical TOC Entry



Right: The chain end-to-end vectors of semicrystalline polymers develop nematic and anti-nematic ordering under tensile and compressive deformations, respectively. Left: The conformations of semicrystalline polymers of length 1000, in the undeformed state and under uniaxial tensile and compressive deformations along the *y*-axis.